AIAA JOURNAL
Vol. 36, No. 4, April 1998

Computation of Flows with Arbitrary Equations of State

Charles L. Merkle*
Pennsylvania State University, University Park, Pennsylvania 16802
Jennifer Y. Sullivan†
GMI Engineering and Management Institute, Flint, Michigan 48504
and
Philip E. O. Buelow‡ and Sankaran Venkateswaran§
Pennsylvania State University, University Park, Pennsylvania 16802

The extension of time-marching computations to fluids with arbitrary equations of state is demonstrated by means of stability analyses, simplified problems, and practical applications. Most of the examples use the properties of supercritical hydrogen for which the density varies by more than an order of magnitude for small changes in pressure and temperature, but representative computations for incompressible fluids and perfect gases are also given to demonstrate the generality of the procedure. Because representative flow velocities in typical supercritical fluids applications are much lower than the speed of sound, convergence enhancement through eigenvalue control is often necessary. This is accomplished through a generalization of earlier preconditioning methods that enables efficient computation of arbitrary equation of state fluids, perfect gases, and incompressible fluids by a single procedure. The present approach thus provides a single method that is uniformly applicable to all equations of state.

Introduction

ALTHOUGH computational techniques are widely used, nearly all applications to date have been limited to one of two equations of state: perfect gases or incompressible fluids. Further, it is generally true that different codes (and frequently distinctly different algorithms) have been employed for these two equations of state. Time-marching techniques[1] have proven to be the method of choice for the computation of perfect gases, especially in the transonic, supersonic, and hypersonic regimes, whereas incompressible computations have been dominated by iterative, pressure-based procedures.[2] Both of these algorithms have been extended to apply to both incompressible and perfect gas flows, but there remains a preponderance of incompressible codes and compressible codes, especially for time-marching algorithms.

The necessity of having to use a different code for each equation of state is a nuisance but, more importantly, there are many fluid dynamic applications for which more general equations of state must be used. Some specific examples include supercritical fluids, refrigerants, and many types of multiphase flows. Engineering applications in the supercritical regime are becoming more prevalent as improved performance causes pressure levels in many applications to be increased. Supercritical fluids exhibit much stronger compressibility than do perfect gases, yet they have very different equations of state. Similarly, applications involving refrigerant fluids are currently popular as manufacturers switch from fluorocarbons to more environmentally friendly fluids. Again, refrigerant fluids require more general equations of state. Finally, multiphase fluid applications can require incompressible fluid assumptions in liquid phase regions and compressible fluid assumptions in vapor regions, again requiring more general capability in the equation of state.

The present paper is aimed at applying a recently developed generalized equation of state algorithm[3] that not only allows these arbitrary equation of state fluids to be computed but also reduces to an incompressible algorithm or a perfect gas algorithm in appropriate limits, thereby unifying all equations of state into a single procedure. The result is a single algorithm and a single code that can be employed for incompressible fluids, perfect gases, or an arbitrary equation of state fluids with similar efficiency in all regimes. Incorporating the method in existing perfect gas codes to extend them to arbitrary equations of state or incompressible flows is quite straightforward.

Presented as Paper 96-0680 at the AIAA 34th Aerospace Sciences Meeting and Exhibit, Reno, NV, Jan. 15–19, 1996; received March 10, 1997; revision received Oct. 16, 1997; accepted for publication Nov. 17, 1997.

*Professor, Propulsion Engineering Research Center; currently Professor, Department of Mechanical Engineering, University of Tennessee Space Institute, Tullahoma, TN 37388. Member AIAA.
†Assistant Professor, Department of Mechanical Engineering. Member AIAA.
‡Postdoctoral Research Associate, Department of Mechanical Engineering, Propulsion Engineering Research Center. Member AIAA.
§Research Associate, Department of Mechanical Engineering, Propulsion Engineering Research Center. Member AIAA.

Equations of Motion for an Arbitrary Fluid

The equations of motion for a general Newtonian fluid with an arbitrary equation of state and variable properties can be written in the familiar conservative form as

$$\frac{\partial \boldsymbol{Q}}{\partial t} + \frac{\partial \boldsymbol{E}}{\partial x} + \frac{\partial \boldsymbol{F}}{\partial y} + \frac{\partial \boldsymbol{G}}{\partial z} = L_v(\boldsymbol{Q}_v) \tag{1}$$

where $\boldsymbol{E}$, $\boldsymbol{F}$, and $\boldsymbol{G}$ represent the inviscid flux vectors and L_v is the diffusive operator. The vectors $\boldsymbol{Q}$, $\boldsymbol{E}$, $\boldsymbol{F}$, and $\boldsymbol{G}$ are

$$\boldsymbol{Q} = \begin{pmatrix} \rho \\ \rho u \\ \rho v \\ \rho w \\ e \end{pmatrix}, \qquad \boldsymbol{E} = \begin{bmatrix} \rho u \\ \rho u^2 + p \\ \rho uv \\ \rho uw \\ (e+p)u \end{bmatrix}$$

$$\boldsymbol{F} = \begin{bmatrix} \rho v \\ \rho uv \\ \rho v^2 + p \\ \rho vw \\ (e+p)v \end{bmatrix}, \qquad \boldsymbol{G} = \begin{bmatrix} \rho w \\ \rho uw \\ \rho vw \\ \rho w^2 + p \\ (e+p)w \end{bmatrix} \tag{2}$$

The diffusive operator is given by

$$\begin{aligned} L_v(\boldsymbol{Q}_v) = {} & \frac{\partial}{\partial x}\left(\boldsymbol{R}_{xx}\frac{\partial \boldsymbol{Q}_v}{\partial x} + \boldsymbol{R}_{xy}\frac{\partial \boldsymbol{Q}_v}{\partial y} + \boldsymbol{R}_{xz}\frac{\partial \boldsymbol{Q}_v}{\partial z}\right) \\ & + \frac{\partial}{\partial y}\left(\boldsymbol{R}_{yx}\frac{\partial \boldsymbol{Q}_v}{\partial x} + \boldsymbol{R}_{yy}\frac{\partial \boldsymbol{Q}_v}{\partial y} + \boldsymbol{R}_{yz}\frac{\partial \boldsymbol{Q}_v}{\partial z}\right) \\ & + \frac{\partial}{\partial z}\left(\boldsymbol{R}_{zx}\frac{\partial \boldsymbol{Q}_v}{\partial x} + \boldsymbol{R}_{zy}\frac{\partial \boldsymbol{Q}_v}{\partial y} + \boldsymbol{R}_{zz}\frac{\partial \boldsymbol{Q}_v}{\partial z}\right) \end{aligned} \tag{3}$$

where the dependent variable is expressed in terms of the primitive variables:

$$\boldsymbol{Q}_v = (p, u, v, w, T)^T \tag{4}$$

and the matrices $\boldsymbol{R}_{xx}$, $\boldsymbol{R}_{xy}$, etc., contain the molecular (or turbulent) viscosities:

$$\boldsymbol{R}_{xx} = \begin{pmatrix} 0 & 0 & 0 & 0 & 0 \\ 0 & \frac{4}{3}\mu & 0 & 0 & 0 \\ 0 & 0 & \mu & 0 & 0 \\ 0 & 0 & 0 & \mu & 0 \\ 0 & \frac{4}{3}\mu u & \mu v & \mu w & k \end{pmatrix}$$

$$\boldsymbol{R}_{xy} = \begin{pmatrix} 0 & 0 & 0 & 0 & 0 \\ 0 & 0 & -\frac{2}{3}\mu & 0 & 0 \\ 0 & \mu & 0 & 0 & 0 \\ 0 & 0 & 0 & 0 & 0 \\ 0 & \mu v & -\frac{2}{3}\mu u & 0 & 0 \end{pmatrix}$$

The remaining matrices may be obtained by appropriate permutation. Note that the first row and the first column of these matrices are zero, ensuring that the diffusion terms in continuity and the diffusion of pressure are zero in the system. In these expressions, ρ represents the density; p is the pressure; u, v, and w are the Cartesian velocity components in the x, y, and z directions, respectively; and μ and k are the viscosity and thermal conductivity. Note we have included the Stokes hypothesis for the second viscosity coefficient.

The total internal energy e is the sum of the internal energy ε, the kinetic energy, and the potential energy

$$e = \rho\left[\varepsilon + \frac{(u^2 + v^2 + w^2)}{2} + gz\right] \tag{5}$$

The enthalpy h is related to the internal energy and the pressure as

$$\rho h = \rho\varepsilon + p \tag{6}$$

and can be defined as a function of any two other thermodynamic properties. Here, we choose the pressure and temperature as the primary dependent variables, so that enthalpy is given by the functional form $h = h(p, T)$. Note that the presence of multicomponent fluids (such as for combustion applications) requires the extension of the enthalpy relation and equations of state to include (for example) the species mass fractions. Similarly, the equation set in Eqs. (2–5) must include additional species relations.

The only place the arbitrary fluid properties explicitly change the formulation is through the equation of state. Accordingly, we specify an arbitrary equation of state that relates the density to the pressure and temperature, $\rho = \rho(p, T)$. This state relation includes the perfect gas law, $\rho = p/RT$, and the incompressible relation, $\rho = \text{const}$, as special cases, but it also allows treatment of any arbitrary fluid that uses the full functional form, as, for example, a supercritical fluid. (Again, combustion calculations require additional variables.) The state relation can be defined in tabular fashion or as a closed-form algebraic relation. In the present paper, our primary attention is on the equation of state for supercritical hydrogen.

Although the use of the conservative flux vectors $\boldsymbol{E}$, $\boldsymbol{F}$, and $\boldsymbol{G}$ is highly important to ensure that global flux conservation is maintained, the dependent variables that appear in Eq. (1) are not necessarily the most convenient for computational purposes. For example, when the enthalpy is a tabular function of the temperature, it is necessary to find the temperature iteratively from the enthalpy, and similarly the pressure can be difficult to infer from the variable Q in Eq. (1). Accordingly, we choose to replace the standard vector Q in the time derivative by the viscous vector $\boldsymbol{Q}_v$ defined in Eq. (4). (Note that $\boldsymbol{Q}_v$ is a unique function of $\boldsymbol{Q}$.) For arbitrary equations of state and reacting flows, this choice makes it possible to compute density and enthalpy directly rather than requiring an iterative inversion of these functions to find T and p.

Having chosen $\boldsymbol{Q}_v$ as the primary dependent variable, we use the chain rule to switch variables:

$$\boldsymbol{\Gamma}_v \frac{\partial \boldsymbol{Q}_v}{\partial t} + \frac{\partial \boldsymbol{E}}{\partial x} + \frac{\partial \boldsymbol{F}}{\partial y} + \frac{\partial \boldsymbol{G}}{\partial z} = L_v(\boldsymbol{Q}_v) \tag{7}$$

where the Jacobian matrix $\boldsymbol{\Gamma}_v = \partial \boldsymbol{Q}/\partial \boldsymbol{Q}_v$ is easily determined by standard procedures:

$$\frac{\partial \boldsymbol{Q}}{\partial \boldsymbol{Q}_v} = \begin{bmatrix} \rho_p & 0 & 0 & 0 & \rho_T \\ u\rho_p & \rho & 0 & 0 & u\rho_T \\ v\rho_p & 0 & \rho & 0 & v\rho_T \\ w\rho_p & 0 & 0 & \rho & w\rho_T \\ h^0\rho_p - (1 - \rho h_p) & \rho u & \rho v & \rho w & h^0\rho_T + \rho h_T \end{bmatrix} \tag{8}$$

Here $\rho_p = (\partial\rho/\partial p)_T$, $\rho_T = (\partial\rho/\partial T)_p$, $h_T = (\partial h/\partial T)_p$, $h_p = (\partial h/\partial p)_T$, and h^0 is the stagnation enthalpy. (Note that h_T is the specific heat at constant pressure.) Other matrices of interest are the Jacobians $\boldsymbol{A}_v = \partial \boldsymbol{E}/\partial \boldsymbol{Q}_v$, $\boldsymbol{B}_v = \partial \boldsymbol{F}/\partial \boldsymbol{Q}_v$, and $\boldsymbol{C}_v = \partial \boldsymbol{G}/\partial \boldsymbol{Q}_v$. The two entries in the top row indicate that the continuity equation contains temporal derivatives of both the pressure and the temperature, which correspond to an expansion of the familiar $(\partial\rho/\partial t)$ term.

The eigenvalues of Eq. (7) determine the convergence rate of any time-marching algorithm. For notational simplicity, we refer only to the x component, although all directions are pertinent. For the x direction, the eigenvalues are obtained from the determinant

$$\left(\boldsymbol{\Gamma}_v^{-1}\boldsymbol{A}_v - \lambda \boldsymbol{I}\right) = 0 \tag{9}$$

which represents a fifth-order polynomial whose roots are readily found to be

$$\lambda = u, u, u, u \pm c \tag{10}$$

where the acoustic speed c is given by

$$c^2 = \frac{\rho h_T}{\rho_T(1 - \rho h_p) + \rho\rho_p h_T} \tag{11}$$

For a perfect gas ($\rho_T = -\rho/T$, $\rho_p = 1/RT$, and $h_T = \gamma R/\gamma - 1$, where γ is the ratio of specific heats), the speed of sound reduces to the familiar relation $c^2 = \gamma RT$. For an incompressible fluid ($\rho_T = \rho_p = 0$), the speed of sound becomes infinite, and the time derivatives in the continuity equation vanish so that it reduces to $\Delta \cdot \boldsymbol{V} = 0$. Again, we emphasize that the form given in Eq. (7) represents the complete Navier–Stokes equations for the several equations of state mentioned earlier.

Eigenvalue Control for Convergence Acceleration

To ensure efficient convergence over all speed ranges and for all equations of state, we replace the physical matrix $\boldsymbol{\Gamma}_v$ in Eq. (7) by a preconditioning matrix $\boldsymbol{\Gamma}_p$, which is chosen to keep all eigenvalues of order unity when nondimensionalized by the particle speed. To retain generality for a wide range of fluids, we choose $\boldsymbol{\Gamma}_p$ in a form analogous to $\partial \boldsymbol{Q}/\partial \boldsymbol{Q}_v$. Specifically, we replace the partial derivatives ρ_p, ρ_T, h_T, and $1 - \rho h_p$ that represent the physical fluid properties by the artificial property terms ρ_p', ρ_T', h_T', and h_p', respectively.[3] With this substitution, the Jacobian $\partial \boldsymbol{Q}/\partial \boldsymbol{Q}_v$ [Eq. (8)] becomes

$$\boldsymbol{\Gamma}_p = \begin{pmatrix} \rho_p' & 0 & 0 & 0 & \rho_T' \\ u\rho_p' & \rho & 0 & 0 & u\rho_T' \\ v\rho_p' & 0 & \rho & 0 & v\rho_T' \\ w\rho_p' & 0 & 0 & \rho & w\rho_T' \\ h^0\rho_p' - h_p' & \rho u & \rho v & \rho w & h^0\rho_T' + \rho h_T' \end{pmatrix} \tag{12}$$

The definition of the preconditioning consists of specifying the four parameters that appear in Eq. (12). Their definition introduces an artificial speed of sound c' that ensures that eigenvalue stiffness is avoided. Additional restrictions on the preconditioning matrix have been given by Peyret and Viviand,[4] Viviand,[5] and Choi and Merkle.[6]

Appropriate forms of these artificial properties can be deduced from perturbation analyses of the equations of motion at low speeds and low Reynolds numbers.[3] The results give

$$\rho'_p = \min(1, Re^2)k_p/V_r^2, \qquad \rho'_T = \min(1, Re/Pr)k_T\rho_T$$
$$h'_T = h_T, \qquad h'_p = 1 - \rho h_p \tag{13}$$

where k_p and k_T are quantities of order unity, V_r is an appropriate reference velocity (typically taken as the local velocity at a grid point), Re is the local cell Reynolds number, and Pr is the fluid Prandtl number. The quantities h'_p and h'_T remain free and have been set to their physical values for convenience. Choosing $k_T = 0$ gives the preconditioning system we have used previously.[6,7] The application to arbitrary equation of state fluids requires that we choose $k_T = 1$. This also has the physical advantage in perfect gas applications that the preconditioned equations approach their exact physical counterparts as the Mach number approaches unity. The advantages of this have been noted by Radespiel et al.[8] Note that, by choosing $\rho'_p = \rho_p$, $\rho'_T = \rho_T$, $h'_T = h_T$, and $h'_p = 1 - \rho h_p$, we return to the nonpreconditioned equations where $\boldsymbol{\Gamma}_p$ becomes the physical Jacobian $\boldsymbol{\Gamma}_v = \partial \boldsymbol{Q}/\partial \boldsymbol{Q}_v$.

The eigenvalues of Eq. (7) are determined by the eigenvalues of $\boldsymbol{\Gamma}_p^{-1}\boldsymbol{A}_v$. Replacing h'_T by h_T and h'_p by $1 - \rho h_p$ as in Eq. (13), the preconditioned eigenvalues become

$$\boldsymbol{\Lambda}_p = \text{diag}\,[u, u, u, u(a + \sqrt{b}), u(a - \sqrt{b})] \tag{14}$$

where the quantities a, b, and d are given by

$$a = \frac{\rho h_T(\rho_p + \rho'_p) + h'_p(\rho_T + \rho'_T)}{2(\rho\rho'_p h_T + \rho'_T h'_p)} \tag{15a}$$

and

$$b = \frac{\rho h_T}{u^2(\rho\rho'_p h_T + \rho'_T h'_p)} + \left[\frac{\rho h_T(\rho_p - \rho'_p) + h'_p(\rho_T - \rho'_T)}{2(\rho\rho'_p h_T + \rho'_T h'_p)}\right]^2 \tag{15b}$$

Here h'_p represents the physical quantity $1 - \rho h_p$, and ρ'_p and ρ'_T represent the preconditioning parameters given in Eq. (13).

In the nonpreconditioned case ($\rho'_p = \rho_p$ and $\rho'_T = \rho_T$), the denominator in Eq. (15) becomes proportional to the speed of sound squared and the quantities in Eqs. (15a) and (15b) reduce to $a = 1$ and $b = c^2/u^2$. Consequently, the last two eigenvalues reduce to $u \pm c$, and we recover the physical acoustic eigenvalues. When the preconditioning given in Eq. (13) is used, the eigenvalues remain well behaved for all conditions, as is demonstrated by the stability and convergence results of the next section.

For an incompressible fluid, $\rho_p = \rho_T = 0$, and the preconditioning in Eq. (13) gives $\rho'_T = 0$. Consequently, the only time derivative remaining in the continuity equation is the time derivative of pressure. The present system thus reduces to the artificial compressibility method of Chorin[9] with ρ'_p replacing the artificial compressibility parameter $(1/\beta)$. In this incompressible case, the quantities a and b in Eq. (15) become

$$a = \frac{1}{2}, \qquad b = \frac{1}{u^2\rho'_p} + \frac{1}{4} \tag{16}$$

which gives the same eigenvalues as the artificial compressibility method.[10,11] This shows that the artificial compressibility method is recovered as a special case of the present procedure.

For compressible flows, the quantities in Eq. (15) take on the form

$$a = \frac{1}{2}\left[1 + \frac{1}{\rho'_p c^2 - (\gamma - 1)}\right] \tag{17a}$$

and

$$b = \frac{c^2/u^2}{\left[\rho'_p c^2 - (\gamma - 1)\right]} + \frac{1}{4}\left[1 - \frac{1}{\rho'_p c^2 - (\gamma - 1)}\right]^2 \tag{17b}$$

which is similar to results used previously for preconditioning in perfect gases.[6,7] (In previous publications we have used $k_T = 0$, whereas here we have used $k_T = 1$.)

Representative applications in which the aforementioned eigenvalue stiffness leads to convergence deterioration include combustion problems in which the flow speeds are small but the density changes are large because of the energy release so that the full compressible equations must be used. (Again, this requires an extension of the equation set to include species equations, but the basic framework remains unchanged.) Similarly, supercritical fluids with heat addition contain dramatic density changes for small changes in temperature, but in many applications the flow velocities are much lower than the speed of sound, and so stiffness again arises in a problem that must be treated as a compressible flow. Finally, incompressible flows in which the acoustic speeds are infinite present insurmountable problems to an unmodified time-marching scheme. The stiffness in all three of these applications is removed by changing the four preconditioning parameters given in Eq. (13). For supersonic flows, where the condition number of the physical matrix is not large, it is sufficient to revert to the physical equations and take $\rho'_p = \rho_p$ and $\rho'_T = \rho_T$.

Stability and Convergence of the Preconditioned Equations

To demonstrate the effectiveness of the generalized equation of state formulation, we compare both stability and convergence results for three different fluids: a perfect gas, an incompressible fluid, and supercritical hydrogen. The equations of state for the first two are well known and can be described by the simple algebraic expressions given earlier. The equation of state for supercritical hydrogen can be represented by a Soave–Redlich–Kwong constitutive property relation.[12] A graphical representation of the density of hydrogen as a function of the temperature is given in Fig. 1 for several values of pressure. The results in Fig. 1 start from the critical pressure, 1.3 MPa, and extend up to 40 MPa, and so all of Fig. 1 is applicable to the supercritical regime. Note that, in the region around 50 K, the density decreases very rapidly with temperature, going from values near 100 kg/m^3 to around 10 kg/m^3 within a few tens of degrees. The rate of change of density with temperature is particularly strong near the critical pressure and temperature and decreases as the pressure and temperature are raised above their critical values.

The properties needed for our generalized formulation of the equations of motion can be interpreted directly from the plot in Fig. 1. The rate of change of density with pressure ρ_p is proportional to the vertical distance between the constant pressure lines. Note that these lines are very widely spaced in the region around 50 K, indicating that ρ_p is quite large there. Similarly, the slope of the constant pressure lines corresponds to ρ_T, the rate of change of density with temperature, and it, too, is large near the critical point. The fact that these properties are nonzero for supercritical hydrogen is a clear indication that the fluid is a compressible medium. Consequently, the adaptation of a density-based, time-marching algorithm

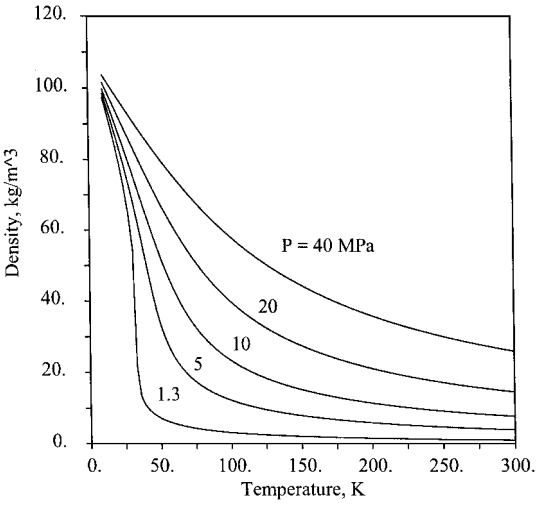

Fig. 1 State relationships for supercritical hydrogen using the Soave–Redlich–Kwong equation of state.[12]

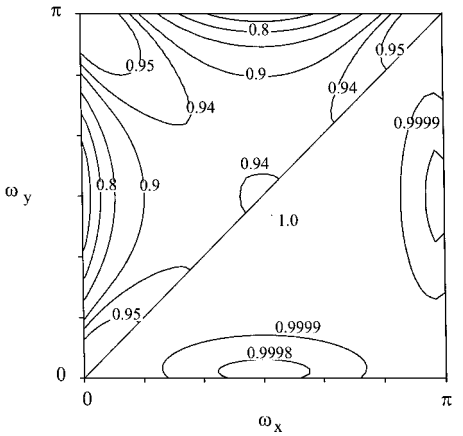

Fig. 2 Stability analysis of ADI algorithm for Euler equations; central differencing, without preconditioning, Courant–Friedrichs–Lewy (CFL) = 3: upper half, perfect gas and $M = 0.7$; lower half, supercritical hydrogen and $u = 4$ m/s.

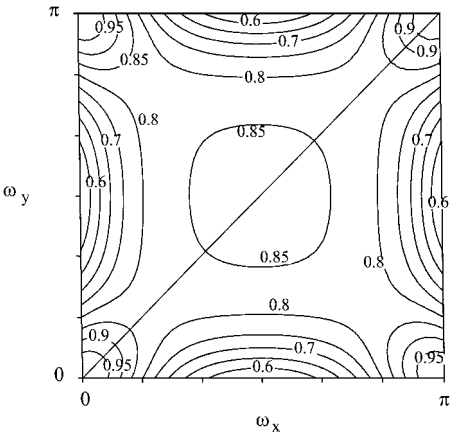

Fig. 3 Stability analysis of preconditioned ADI algorithm for Euler equations, CFL = 3: upper half, supercritical hydrogen, $T = 50$ K, $p = 5$ MPa, and $u = 4$ m/s; lower half, incompressible flow and $u = 4$ m/s.

would appear to be straightforward. Nevertheless, the application of time-marching methods to typical supercritical hydrogen problems results in very slow convergence. The reason stems from the wide disparity between the characteristic velocities in such applications. It is for this reason that the generalized preconditioning described earlier is necessary. These effects are most readily explained by considering the stability characteristics for a representative algorithm.

As a representative example of the effect of the equation of state on the stability characteristics, we consider the Euler equations. To put the stability results into perspective, we first compare results for a perfect gas with those for supercritical hydrogen when the full physical variables are used in the time derivative (no preconditioning). For definiteness, we use central differencing in space and alternating direction implicit (ADI) approximate factorization in time[1] and present the magnitude of the spectral radius of the amplification matrix obtained from a classical von Neumann analysis of the Navier–Stokes equations.

Stability results for the nonpreconditioned equations for a perfect gas are given in the upper half of Fig. 2, whereas similar results for supercritical hydrogen are given in the lower half. [These nonpreconditioned results correspond to using $\rho'_p = \rho_p$, $\rho'_T = \rho_T$, $h'_T = h_T$, and $h'_p = 1 - \rho h_p$ in the preconditioning matrix Γ_p of Eq. (12).] The stability results for the perfect gas are computed for a flow Mach number of 0.7 and a flow angle of 45 deg ($v/u = 1$), whereas those for supercritical hydrogen are for a velocity of 4 m/s, a temperature of 50 K, a pressure of 5 MPa, and the same flow angle. (Note that Mach number is not a very suitable parameter for a liquid-like supercritical fluid, and so the fluid velocity is specified.) As can be seen, the amplification factors for the perfect gas (upper half of Fig. 2) are reasonable, with damping rates of around 0.9 over most of the mid-wave-number range and lower values along the coordinate axes except in the corners where the amplification factor goes to unity. These high-wave-number peaks are easily removed by a small amount of artificial dissipation, so that, overall, these stability characteristics should provide reasonably good convergence.

The stability results for the hydrogen application (lower half of Fig. 2) are, however, much different. Here, the amplification factor is nearly unity (0.9999) over almost the entire wave-number region, and the resulting convergence can be expected to be very slow. The reason for this very strong difference is that the Mach number in the supercritical hydrogen is only $M = 0.01$. (The speed of sound at these conditions is $c = 400$ m/s.) Low-Mach-number conditions are widely known to provide very stiff eigenvalues and very slow convergence. In fact, analysis of the stability relation for Euler equation applications of any generalized fluid shows that the stability characteristics depend only on the flow angle and the Mach number no matter what equation of state is used. The difficulty is that the Mach number is not typically considered as a parameter in supercritical fluid applications where the velocities are almost always much lower than the speed of sound. Still, time-marching methods rely on acoustic waves to remove errors during the convergence process, so that Mach number is a primary parameter in computations. Efficient convergence requires that something must be done to rectify the stiffness that is so encountered. It is for this reason that we have introduced the preconditioning matrix in Eq. (12).

The effects of preconditioning for this simple case are quite dramatic as shown by the amplification factors for the supercritical hydrogen case in the upper half of Fig. 3. In these preconditioned stability results, the parameter ρ'_p has been replaced by $\rho'_p = k_p / V_r^2$ with $k_p = 1$ and $\rho'_T = \rho_T$ ($k_T = 1$). This simple change makes the stability characteristics for the supercritical hydrogen case look quite good. In fact, they become somewhat more favorable (that is, the amplification factors are slightly lower) than those for the nonpreconditioned $M = 0.7$ perfect gas case. (Compare with the upper half of Fig. 2.) The mid-wave-number amplification factors are in the 0.85 range, with sharp falloff along the axes (except at the corners) promising efficient convergence. As shown later, this promise is realized in computations.

The curve in the lower half of Fig. 3 shows the result of preconditioning the incompressible equations by the same procedure. This preconditioning converts the incompressible equations to the traditional artificial compressibility formulation,[9] but it does so in a manner that treats incompressible flow as a special case of an arbitrary equation of state. (As noted earlier, for the incompressible case ρ'_p corresponds to the traditional artificial compressibility parameter $1/\beta$.) The stability characteristics for preconditioned incompressible flow are essentially identical to those for hydrogen even though the physical properties ρ_p and ρ_T are both zero. Further, when this preconditioning is applied to the $M = 0.7$ perfect gas case in the upper half of Fig. 2, it, too, becomes identical to these results, indicating that the preconditioning also works for perfect gases. Companion perfect gas stability results for Mach numbers ranging from 10^{-5} to transonic verify that the preconditioned amplification factors remain essentially the same for all speeds. Consequently, whereas stability characteristics for Euler solutions are a function of Mach number only for all equations of state, including incompressible flow, the stability characteristics of the preconditioned system are essentially the same for all Mach numbers and all equations of state and depend only on the flow angle. These examples demonstrate the ease with which the stiffness in the Euler equations can be removed for arbitrary speeds and arbitrary equations of state.

To demonstrate the significance of these stability results, we apply them first to a simple flowfield. We consider the inviscid flow of an arbitrary fluid in a straight duct at a Mach number of 0.01 and look at the convergence from an initial condition corresponding to a small random perturbation from the exact (uniform flow) solution. Although this problem appears trivial, the return to uniform flow at low Mach numbers takes tens of thousands of iterations without preconditioning. With preconditioning, it converges very rapidly as is shown later.

Three cases are considered: 1) a perfect gas, 2) an incompressible flow, and 3) supercritical hydrogen at 5 MPa and 50 K. Figure 4 displays the convergence histories for each of these cases. (The

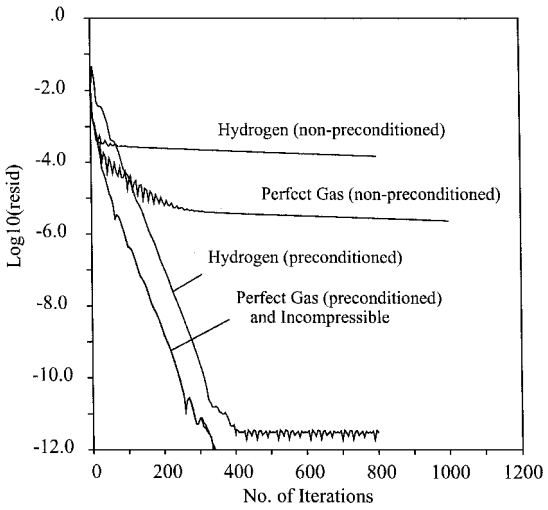

Fig. 4 Convergence of flow in an inviscid straight duct at $M = 0.01$ for supercritical hydrogen, perfect gas, and incompressible flow using the original equations and the preconditioned equations.

addition of preconditioning has a negligible effect on CPU time per iteration, and so comparisons of the number of iterations correspond to relative CPU times.) It is evident that without preconditioning the convergence quickly deteriorates, and more than 10,000 iterations are required to reach a machine-accurate solution. When preconditioning is employed, all three cases converge at the same rate, reaching machine accuracy in fewer than 400 iterations. The convergence therefore correlates with the stability analyses and indicates that the preconditioning works equally well for the Euler equations regardless of the equation of state. Next we look at applications of both the Euler and Navier–Stokes equations to more practical problems using examples based on the equation of state of hydrogen.

Representative Solutions for Practical Problems

The ultimate proof of convergence enhancement must rest upon demonstration of its effectiveness in practical problems. In this section, we present some representative results to demonstrate the capabilities. Figure 5 shows a representative result for inviscid flow of supercritical hydrogen through a two-dimensional cascade. The flow conditions correspond to 5 MPa and 100 K where the speed of sound is 800 m/s. The inlet velocity is 240 m/s. A 121×41 stretched grid was used. The contours in the figure correspond to the perturbation pressure. The convergence histories with and without preconditioning are given in Fig. 6. (Again, CPU times scale with iteration number for all cases.) This case was also run as a perfect gas and an incompressible flow at the same conditions, and these results are also included in Fig. 6. The improvement with preconditioning is not as significant as was observed in Fig. 4 because the Mach number is larger for this case; however, uniform convergence is again obtained for each of the three fluids.

As a second example, we consider the laminar flow of hydrogen through a heated, rectangular duct at a Reynolds number of 1×10^3. The duct hydraulic diameter is 1.5 mm, which, at this Reynolds number, corresponds to velocities that far negate the effects of buoyancy. A schematic of the configuration is shown in Fig. 7. The incoming hydrogen is at a temperature of 40 K and a pressure of 10 MPa. The wall temperature on one of the narrow sides of the rectangle is set to 300 K, whereas that on the opposite side is kept at the fluid temperature of 40 K. A linear variation between these two temperatures is specified on the side walls. As noted in Fig. 7, the duct length is 20 hydraulic diameters. A grid with approximately 300,000 points was used with moderate stretching near the walls. The variation in density resulting from the heating results in a much different flowfield and considerably different heat transfer than in the case of a constant property fluid. Our interest in this problem arises from the regenerative cooling of rocket combustion chambers, but here we use this problem as an example of the application of computational techniques to an arbitrary equation of state fluid.

An overview of the axial variation of the flowfield on the midplane of the duct is given in the lower portion of Fig. 7. The top

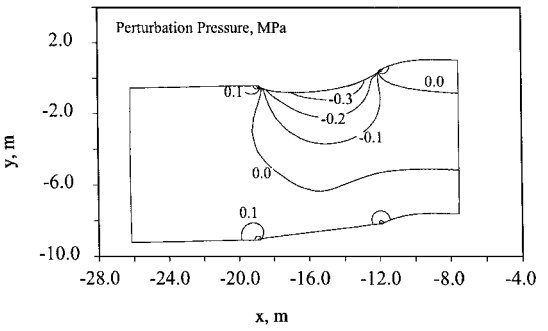

Fig. 5 Contours of perturbation pressure for flow of supercritical hydrogen through a two-dimensional cascade; $u = 240$ m/s, $p = 5$ MPa, and $T = 100$ K.

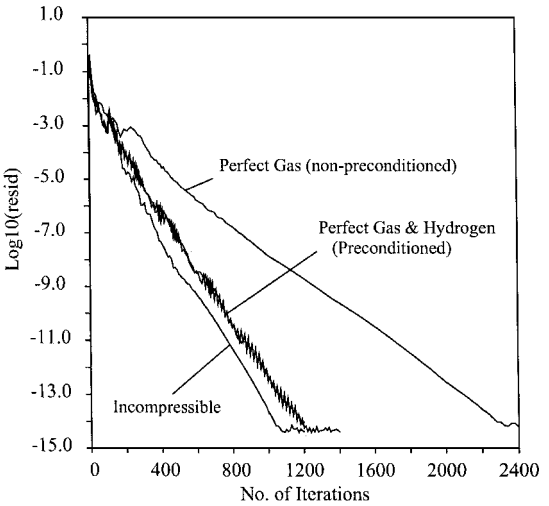

Fig. 6 Convergence rates for inviscid flow through a two-dimensional cascade for supercritical hydrogen, incompressible flow, and perfect gas. Results are shown for both the original equations and the preconditioned equations.

wall is at the fluid temperature, and the bottom wall is heated to 300 K. Figure 7 includes contours of the density, the temperature, and the axial velocity as well as velocity vectors showing the cross-stream profiles. The temperature and density contours clearly show the thermal boundary layer that develops on the bottom wall. The thickness of this boundary layer, however, is accentuated by the thermal expansion of the hydrogen as it is heated. The dramatic change in density induces a fairly strong upward velocity in the cross plane (shown later) that displaces the boundary layer toward the opposite wall. The velocity vectors also show that the heated flow near the wall accelerates so that the peak velocity occurs near the bottom wall, and the profile is highly nonsymmetric. The velocity contours demonstrate that the heating causes a substantial flow acceleration that is far larger than is seen in the constant property case. As a result, the pressure drop in the duct is several times greater than that in a similar flow of a constant property fluid.

A better understanding of the flowfield can be obtained by looking at the property contours in the cross plane. Some representative results are given in Fig. 8, corresponding to an axial location halfway through the duct, $x/D_h = 10$. Figure 8 shows the cross-stream velocity, along with contour plots of the axial velocity, temperature, and density. The heated wall is on the bottom, and taking advantage of symmetry, only half of the duct is shown. Looking first at the density and temperature contours, it is seen that the warmer fluid near the bottom has expanded by a factor of about 5 compared with the nonheated fluid. This expansion is responsible for displacing the fluid away from the bottom wall, as was noted in conjunction with Fig. 7. This thermal expansion of the fluid also causes a fairly strong streamwise vortex to develop in the cross plane, as is seen in the plot at the left in Fig. 8. This vorticity arises because of the $\nabla\rho \times \nabla p$ term that is present in this highly compressible flow. The generation of streamwise vorticity in a constant property fluid in a

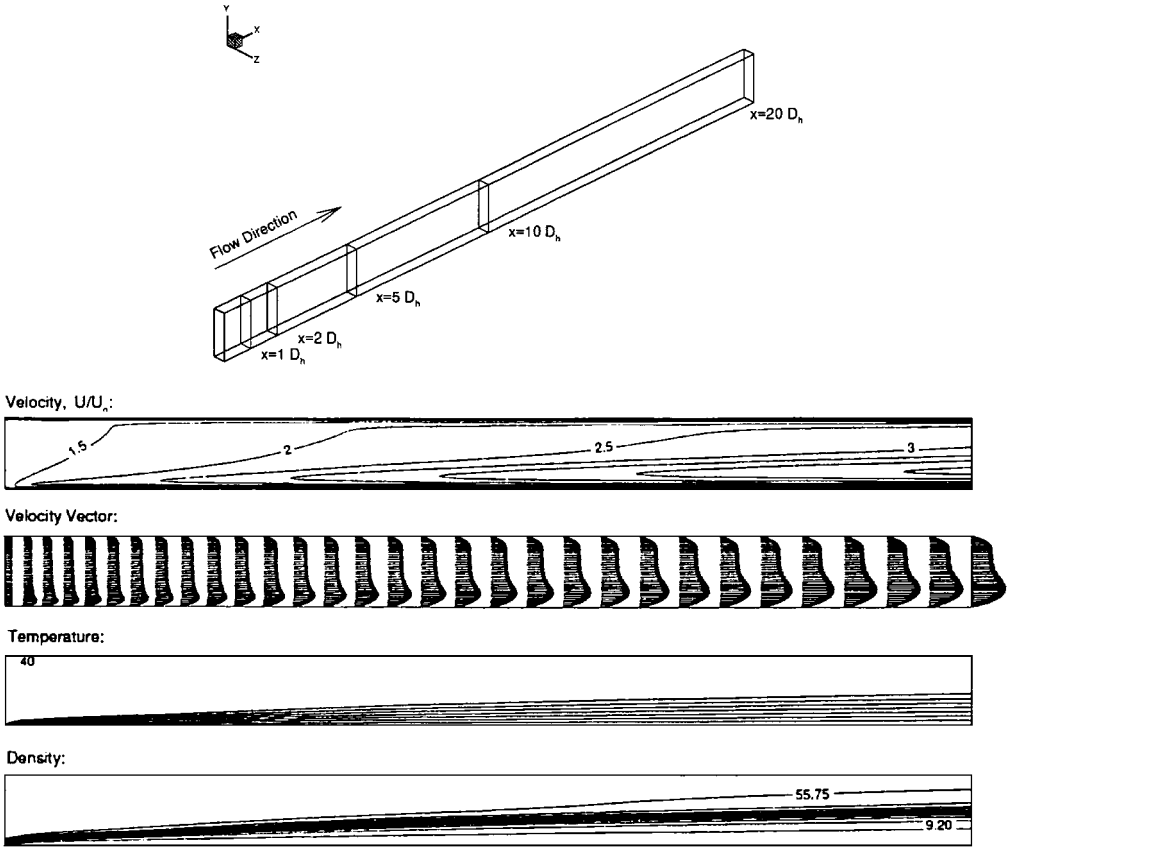

Fig. 7 Velocity, density, and temperature on midplane of rectangular duct as a function of axial distance.

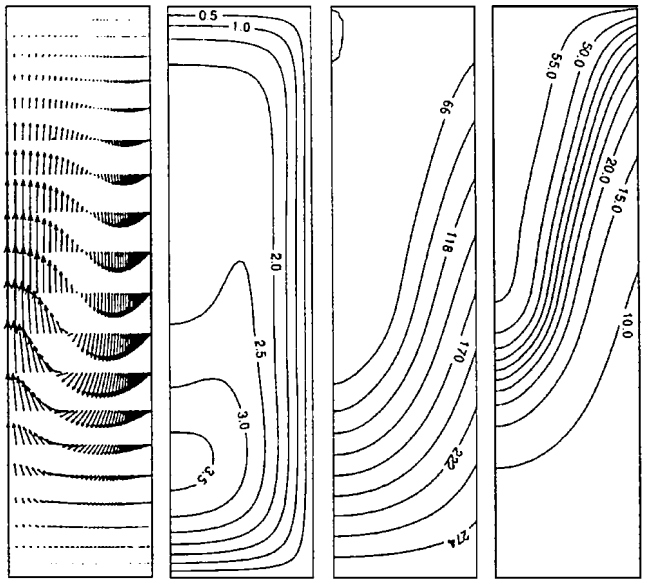

Fig. 8 Velocity, density, and temperature contour plots in cross plane of rectangular duct, $x/D_h = 10$. The temperature is given in Kelvins, and the density in kilograms per cubic meter. The velocity is nondimensionalized by the bulk velocity U_0.

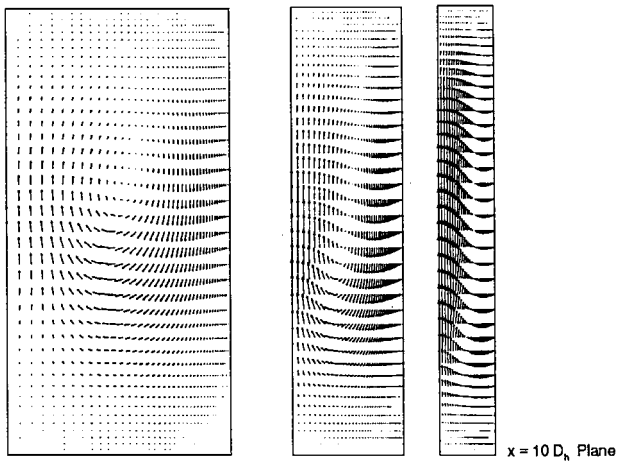

Fig. 9 Cross-stream velocity vectors for duct aspect ratios 1, 2, and 4; $x/D_h = 10$.

straight tube is clearly not possible. This relatively strong flow in the cross plane has a considerable effect on the heat transfer, as it removes the heated flow from the bottom wall and replaces it with fresh, unheated fluid, thereby enhancing the heat transfer. Finally, the axial velocity contours in Fig. 8 show that the peak velocity occurs near the bottom of the duct where the fluid expansion has the most impact, as was noted from the axial profiles of Fig. 7.

The effects of duct aspect ratio on the velocity pattern in the cross plane are shown in Fig. 9. For these computations, the Reynolds number based on the hydraulic diameter was held constant. Here, duct aspect ratios of 1 (a square), 2, and 4 are presented. The results show the velocity in the cross plane at the $x/D_h = 10$ station. As can be seen, vorticity is present for all duct aspect ratios, but the larger-aspect-ratio ducts pinch the vortex so that its aspect ratio fits that of the duct. Computations at duct aspect ratios higher than 4 indicate that the single pair of vortices (obtained by reflecting the plots in Fig. 9 about the symmetry plane) becomes broken up into two pairs, one above the other. These results clearly show the importance of including variable property effects in the computations.

Conclusions

The effectiveness of a unified preconditioning method for arbitrary equation of state fluids has been demonstrated by means of stability theory, simplified problems, and realistic applications. As a primary example of the effectiveness of the method, applications to flows of supercritical hydrogen have been made. In addition, both

perfect gas cases and incompressible flows have been considered to demonstrate generality. Further, it has been shown that the method simplifies to Chorin's artificial compressibility method for the incompressible case.

Stability results show that in the Euler equation limit the convergence of a given time-marching algorithm depends only on the flow angle and the Mach number. Thus, even though the Mach number is seldom considered as a parameter in liquid-like, supercritical flows because the velocity is so much lower than the speed of sound, it remains a dominant parameter in determining the convergence of time-marching computations. This low-speed stiffness is removed by replacing the physical thermodynamic properties in the time derivatives of the equations of motion by artificial properties. The resulting preconditionedequations are shown to have stability characteristics that are independent of the Mach number and depend only on the flow angle for all equations of state. The particular set of artificial properties that is chosen is shown to reduce to the familiar artificial compressibility formulation for incompressible flow. The applicability of these stability results is then demonstrated by computing simple problems for which the convergence rate in supercritical hydrogen is shown to be identical to that of both perfect gases and incompressible flow.

Practical computations of supercritical hydrogen are then shown to ensure that the findings from stability theory and simplified problems can be extended to realistic applications. The flow of supercritical hydrogen through a two-dimensional cascade is shown to converge efficiently and to provide accurate solutions. Three-dimensional, viscous solutions of the flow of supercritical hydrogen in a straight rectangular duct with heat addition from one wall indicate that the compressibility of the hydrogen introduces streamwise vorticity in a manner analogous to that observed in a curved duct. The resulting vortices have an important effect on the heat transfer. The compressibility of the fluid also leads to strong acceleration of the fluid, increasing the pressure drop.

Acknowledgments

This work was supported under NASA Grants NAGW-1356, NAS 8-3886, and NCC 8-46 from the NASA Marshall Space Flight Center.

References

[1] Briley, W. R., and McDonald, H., "On the Structure and Use of Linearized Block Implicit Schemes," *Journal of Computational Physics*, Vol. 34, No. 1, 1980, pp. 54–73.

[2] Harlow, F. H., and Welch, J. E., "Numerical Calculation of Time-Dependent Viscous Incompressible Flow with Free Surfaces," *Physics of Fluids*, Vol. 8, No. 12, 1965, pp. 2182–2185.

[3] Merkle, C. L., "Preconditioning Methods for Viscous Flow Calculations," *Computational Fluid Dynamics Review 1995*, edited by M. Hafez and K. Oshima, Wiley, Chichester, England, UK, 1995, pp. 419–436.

[4] Peyret, R., and Viviand, H., "Pseudo-Unsteady Methods for Inviscid or Viscous Flow Computation," *Recent Advances in the Aerospace Sciences*, edited by C. Casci, Plenum, New York, 1985, pp. 41–71.

[5] Viviand, H., "Pseudo-Unsteady Systems for Steady Inviscid Calculations," *Numerical Methods for the Euler Equations of Fluid Dynamics*, Society for Industrial and Applied Mathematics, Philadelphia, 1985, pp. 334–368.

[6] Choi, Y. H., and Merkle, C. L., "The Application of Preconditioning to Viscous Flows," *Journal of Computational Physics*, Vol. 105, No. 2, 1993, pp. 207–223.

[7] Buelow, P. E. O., Venkateswaran, S., and Merkle, C. L., "Grid Aspect Ratio Effects on the Convergence of Upwind Schemes," AIAA Paper 95-0565, Jan. 1995.

[8] Radespiel, R., Turkel, E., and Kroll, N., "Assessment of Preconditioning Methods," Institut für Entwurfsaerodynamik der DLR, 95-29, Braunschweig, Germany, 1995.

[9] Chorin, A. J., "A Numerical Method for Solving Incompressible Viscous Flow Problems," *Journal of Computational Physics*, Vol. 2, 1967, pp. 12–26.

[10] Rogers, S. E., Kwak, D., and Kiris, C., "Numerical Solution of the Incompressible Navier–Stokes Equations for Steady-State and Time-Dependent Problems," AIAA Paper 89-0463, Jan. 1989.

[11] Choi, D., and Merkle, C. L., "Fully Implicit Solution of Incompressible Flows," *AIAA Journal*, Vol. 23, No. 10, 1985, pp. 1518–1524.

[12] Oefelein, J. C., and Yang, V., "Simulation of High-Pressure Spray Field Dynamics," *Recent Advances in Spray Combustion: Spray Combustion Measurements and Model Simulation*, Vol. 2, edited by K. K. Kuo, Vol. 171, Progress in Astronautics and Aeronautics, AIAA, Reston, VA, 1996, pp. 263–304.

J. Kallinderis
Associate Editor